Moroccan heated clay-based geopolymer reinforced with date palm cellulose: Microstructure characterization and mechanical/physical properties

Abdellah Mourak, Mohamed Hajjaji

Laboratoire des Sciences des Matériaux et Optimisation des Procédés, Faculté des Sciences Semlalia, Université Cadi Ayyad, B.P. 2390, Av. Pce My Abdellah, Marrakech 40001, Morocco.

Abstract

The objective was to study the cellulose addition effect on the geopolymerization of heated clay. The clay, composed of illite, plagioclase and kaolinite, was heated at 700°C for 2 hrs and mixed with cellulose (up to 10 mass%). The mixtures were NaOH-activated, and shaped samples were aged at 83°C for 30 days. The cured samples were investigated by using XRD, FT-IR spectroscopy and SEM. The influence of the cellulose addition on the mechanical/physical properties was also evaluated. The results showed that zeolite ZK-14, hydrosodalite, sodium carbonate, and geopolymer composed of poly(sialate) units were formed in all cured samples. The relative amounts of zeolite and metakaolin evolved antagonistically, while that of illite slightly decreased with the increase of cellulose content. Metakaolin and illite were involved in the geopolymerization process. Cellulose addition led to the improvement of the flexural strength of the samples (~1.2 MPa / (mass% cellulose)), and to the porosity reduction. In contrast, the water absorption was increased (~ 2.3 % / (mass% cellulose)). The positive effect of cellulose on samples performances was explained on the basis of hydrogen bonding between the functional moieties of cellulose and the active sites of samples constituents, namely zeolites, metakaolin, illite and geopolymer. As filler, zeolite likely contributed to the samples strengthening, and the detrimental impact of Na-carbonate was insignificant. Based on the results obtained, the composites could be used as binders for bricks manufacturing, or as lightweight mortars.

Keywords: Heated clay, geopolymer, cellulose, microstructure, sample performances.

Mineralogical Society

This is a 'preproof' accepted article for Clay Minerals. This version may be subject to change during the production process.

DOI: 10.1180/clm.2024.6

https://doi.org/10.1180/clm.2024.6 Published online by Cambridge University Press

1. Introduction

Recently, major concern has been expressed regarding Ordinary Cement Portland (OPC) manufacturing because of the huge amount of carbon dioxide release (Zhang et al., 2023), the energy required and the scarcity of the geomaterials needed. So, a worldwide research activity has been undertaken to find out eco-friendly cementitious materials with good physical and mechanical properties (Mohamad et al., 2022; da Silva Rego et al., 2023; Shi et al., 2023). Geopolymers, which are low-temperature synthesized aluminosilicates, have been considered as potential alternatives for OPC (Ayub and Khan, 2023; Ranjbar et al., 2020; Giacobello et al., 2022; Tanu et al., 2022; Jwaida et al., 2023). Fly ash, calcined clays, volcanic ash and blast furnace slag are among the used aluminosilicate sources for geopolymers synthesis. For the latter purpose, these materials are dissolved by moderate to strong alkaline solutions (4-12 M). NaOH is by far the most used alkali-hydroxide activator. Mixtures of NaOH and Na_2SiO_3 are also used. In the latter condition, OH^- ions (NaOH-derivative species) are involved in the dissolution of the aluminosilicate whilst sodium silica plays a role of binder (Mijarsh et al., 2015). Na^+ ions contribute to the charge balance as well as to zeolite formation. The excess of Na^+ ions induces the formation of carbonate by reaction with the atmospheric carbon dioxide. Such a phenomenon occurs particularly in the case of NaOH-activated metakaolin system (Valentini, 2018).

Considering for instance metakaolin, which is considered as a high-grade source material for geopolymer synthesis, the alkali-activation resulted in the formation of $Al(OH)_4^-$, $H_3SiO_4^-$ and $H_2SiO_4^{2-}$species (Valentini, 2018; Weng and Sagoe-Crentsil, 2007) together with a sodium aluminosilicate hydrate (Na_2O-Al_2O_3-SiO_2-H_2O gel) (Valentini, 2018). Referring to Weng and Sagoe-Crentsil (2007), the association of $Al(OH)_4^-$ and $H_2SiO_4^{2-}$ results in the formation of small oligomers (dimers and trimers). However, the condensation between $Al(OH)_4^-$ and $H_3SiO_4^-$ leads to polymers and larger oligomers. The latter products consist of linked silica ($[SiO_4]^{4-}$) and alumina ($[AlO_4]^{4-}$) tetrahedral. The three-dimension structure obtained is called geopolymers (Van Deventer et al., 2077; Almutairi et al., 2021; Sotelo-Piña et al., 2019).

Preprinted Article

https://doi.org/10.1180/clm.2024.6 Published online by Cambridge University Press

Cellulose is one of the main constituents of plants. It exists as fibers and has a polymeric structure. The cellulose chains are composed of β-D-glucose units, and their organization into sheets is essentially achieved by the methylol (-CH_2OH) and the hydroxyls moieties (Etale et al., 2023; Bashline et al., 2014). Cellulose fibers have high ratio strength/density (Chen et al., 2021; Emenike et al., 2023). Therefore, they are proven to be suitable to reinforcing some matrix materials (Ferreira et al., 2021; Zheng et al., 2023; Mourak et al., 2021; Lazorenko et al., 2022). The cellulose reinforcing capability is mainly influenced by the fiber dimensions, surface properties and moisture retention (Farhan et al., 2021; Santana et al., 2021). Referring to some authors, the cellulose addition to the cementing materials should be limited (0.2-2.0% v/v) (Jamshaid et al., 2022; Raghunath et al., 2022; de Souza et al., 2023; dos Reis et al., 2023). The addition of high amounts of cellulose resulted in water adsorption increase, and consequently the mechanical strength of the cellulose-containing cementing materials dropped (Singh and Gupta, 2020; Jaberizadeh et al., 2022).

The reinforcing effect of the cellulose fibers can be improved by alkali-activation using NaOH solutions (18-32 mass %) at 25-40°C. Due to the chemical treatment, fibrils with large surface area and high aspect ratio form, and consequently the adhesion between the reinforcing material and the matrix is enhanced (Aravindh et al., 2022; Asyraf et al., 2022).

Considering the above literature data, this work of research, which aimed to investigate the microstructure and determine the mechanical/physical properties of heated-clay-based geopolymer samples, has fundamental and application interests. Regarding the latter interest, this work is a contribution to the development of eco-friendly-clay based building material with acceptable performances. The raw materials (clay and palm date rachis) used are globally found and the product preparation process does not need sophisticated plants or much energy as for OPC manufacturing (Semugaza et al., 2023). Fundamentally, this study is a contribution to the understanding of the chemical interactions, which could occur between cellulose functional moieties and active sites of geopolymer and associated aluminosilicates (zeolite, illite and metakaolin).

2. Materials and methods

2.1. Clay material and cellulose

The raw clay material was from Kharrou Mountain (Rehamna, Morocco). It was essentially composed of mica/illite, pyrophyllite, kaolinite, plagioclase, and calcite (Figs.1

Preprinted Article

https://doi.org/10.1180/clm.2024.6 Published online by Cambridge University Press

&2). As an aluminosilcate-rich material (Table 1), the clay seemed to be suitable as a precursor for geopolymers preparation. So, the clay was the object of mechanical and heating treatments, as detailed below. As a result of heating, kaolinite was vanished and metakaolin was formed (Figs. 1&2), whereas illite resisted heating as its structure is breakdown at T > 900°C (Altieri and Ferrari, 2006). As can be deduced from the thermograms given in Fig. 3, kaolinite was the object of dehydroxylation at about 523°C. In this respect, it should be noted that the DTA curve showed endothermic phenomena at about 88 and 272°C, which were assigned to the losses of hygroscopic and strongly retained waters. The weak endothermic peak at 812°C was associated with calcite decomposition.

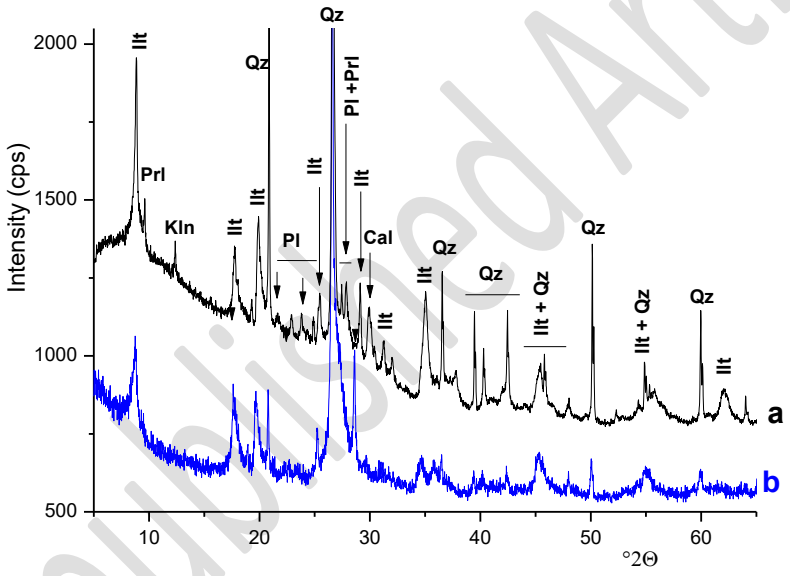

Fig.1. X-ray diffraction traces of the raw (a) and heated (b) clay.
Qz:Quartz (PDF# 05-0490), Kln:Kaolinite (PDF# 83-0971), IIt: Illite (PDF# 43-0685), Prl: Pyrophyllite(PDF# 96-0277), cal:Calcite(PDF#83-1762), Pl: Plagioclase (PDF# 41-1486).

Preprinted Article

https://doi.org/10.1180/clm.2024.6 Published online by Cambridge University Press

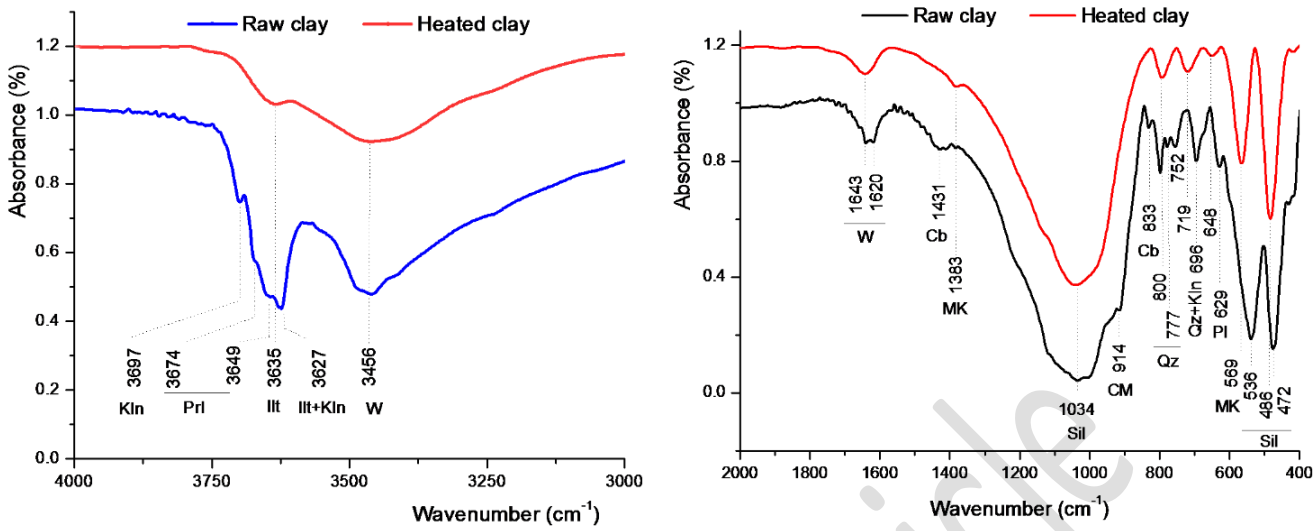

Fig. 2. FT-IR spectra of the raw and heated clay.
Qz:Quartz, Kln:Kaolinite, MK:Metakaolin, Sil:Silicates, Ilt: Illite, W:Water, cb: Carbonates, Prl:Pyrophyllite, Pl: Plagioclase,W: Water, CM : Clay minerals.

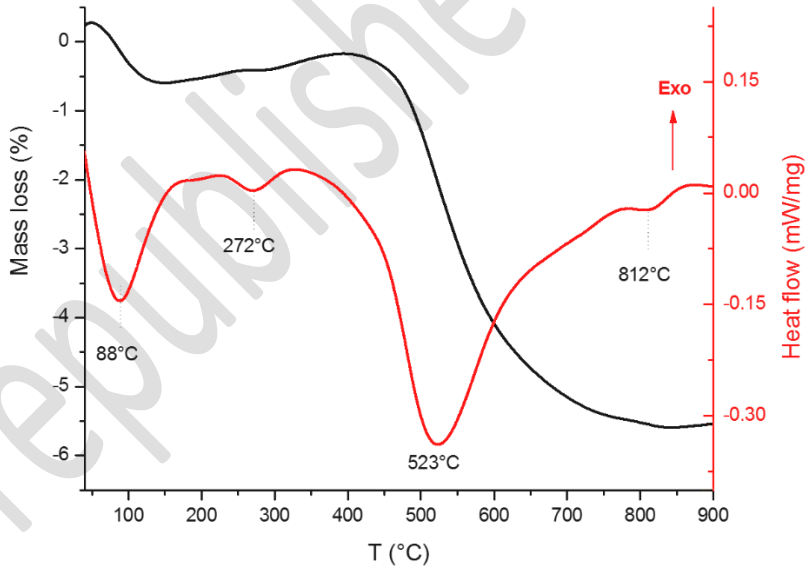

Fig.3. Thermal curves (TG, DTA) of the raw clay.

The cellulose used as reinforcement was extracted from the date palms (Phoenix dactylifera) rachis, following the steps shown in Fig. 4. More details regarding the cellulose extraction are given below. The physical characteristics of the isolated cellulose, which manifested as shown in Fig. 5, are provided in Table 1.

Prepublished Article

https://doi.org/10.1180/clm.2024.6 Published online by Cambridge University Press

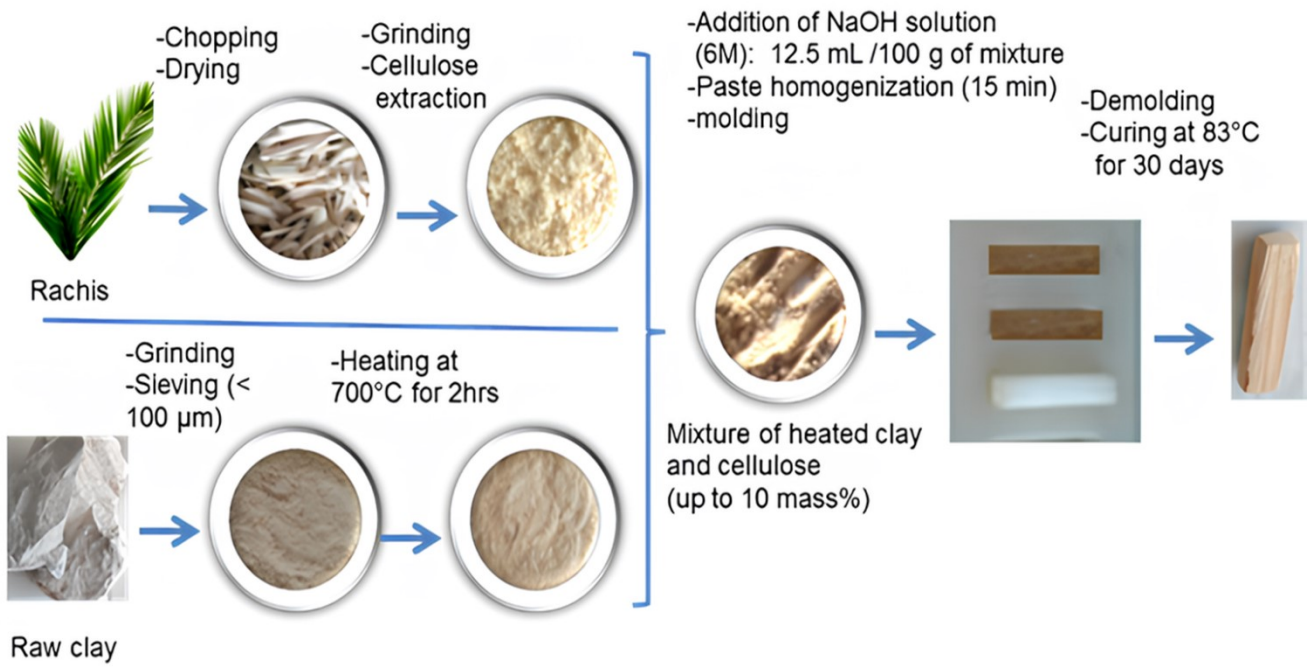

Fig. 4. Main steps followed for date palm rachis and raw clay treatments, and experimental operations for heated clay-cellulose samples preparation.

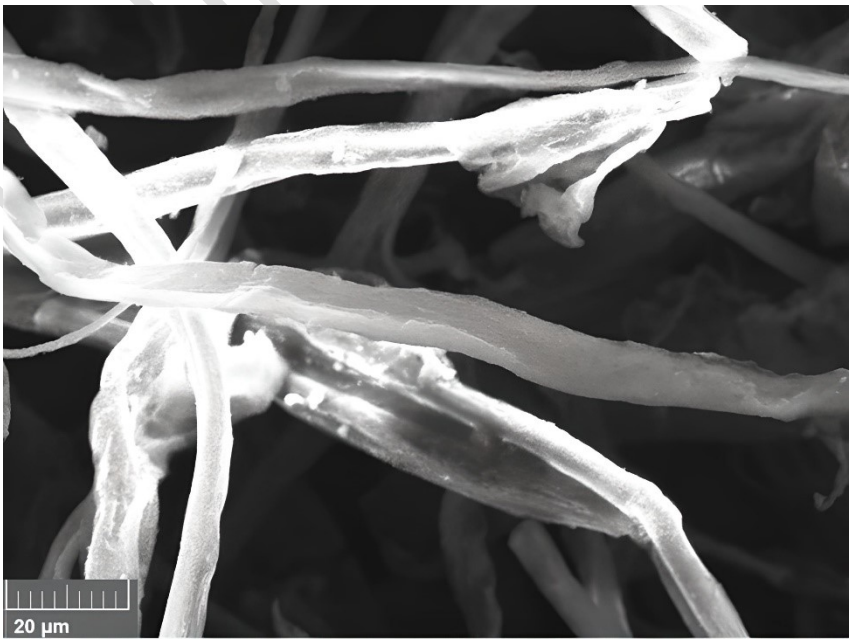

Fig. 5. SEM micrograph showing the cellulose fibers morphology.

Preprint

https://doi.org/10.1180/clm.2024.6 Published online by Cambridge University Press

Table 1. Chemical composition (mass%) of the used clay, the relative amounts of the date palm rachises constituents, and the physical characteristics of the extracted cellulose.

Clay								
SiO_2	Al_2O_3	TiO_2	Fe_2O_3	MnO	MgO	K_2O	CaO	Na_2O
56.75	33.74	1.80	1.24	0.01	0.58	2.50	0.27	1.76
Date palm rachises constituents								
Lignin		Hemicellulose		Cellulose		Balance		
20		30.5		47.5		2		
Physical characteristics of the extracted cellulose								
Crystallinity index (%)		Average molecular weight (g/mol)		Polymerization degree				
67		144622		892				

Preprinted Article

2.2. Samples **preparation**

For geopolymer synthesis, dried portions of the clay heated at 700°C for 2 hrs and cellulose (10 mass%) were introduced in a glass container and mixed for 15 min. The blend was transferred into a plastic bag and mixed with NaOH solution (6 M). The optimal ratio (NaOH solution volume) / (blend weight) was of 12.5 mL/100 g. The paste was kneaded for 15 min (time to obtain a plastic paste), and the shaping operation was manually accomplished in about 20 min. The shaped samples (3.8x9.2x40 mm) were placed in a Memmert oven and aged at 83°C for 30 days. The oven used was functioning in open air. In relation with the adopted curing conditions, it can be noted that referring to Mo Bing-hui et al. (2014), the increase of the curing temperature (up to 100°C) accelerates the dissolution, polymerization, reprecipitation processes of the geopolymerization reaction. Therefore, the physical/mechanical properties of the product are enhanced. The effect of the curing time on the geopolymerization is still under debate (Heah et al., 2014; Van Jaarsveld et al., 2022).The NaOH-activation solution was prepared by dissolution of NaOH pellets (Sigma-Adrich product, purity: > 97.0%) in distilled water.

2.3. Experimental procedures and instruments

https://doi.org/10.1180/clm.2024.6 Published online by Cambridge University Press

The raw clay was crushed and ground using an agate mortar, then passed through a 100 µm sieve. The sieve fraction was heated in a Nabertherm furnace. The heating conditions were as follows: heating rate: 7°C/min, maximum temperature: 700°C, soaking time: 2 hrs, atmosphere: air.

For cellulose extraction, the pigments and lipids associated with cellulose were removed by using anazeotropic mixture of ethanol and toluene. The solvent extraction was performed by using a conventional Soxhlet extractor. The hemicelluloses and lignin were eliminated with a solution of sodium hydroxide (2 mass%), and heating at 80°C for 2 hrs. The fiber bleaching was done with a solution of sodium chlorite (1.7% w/v) at 70 °C (Mourak et al., 2021).

The polymerization degree (PD) of the extracted cellulose was calculated by using the equation:

$$PD = (AMW)/M_C$$

(AMW is the average molecular weight (144622 g/mol); M_C is the molecular weight of cellulose (162.14 g/mol). AMW was measured following the procedure detailed elsewhere (Evans et al., 1989; Malešič et al., 2021).

As compared with the literature data (Hallac and Ragauskas, 2011), the PD obtained was between low and moderate values. It was believed that the cellulose extracted, with such a PD value, can be used without significant agglomeration tendency.

The crystallinity index (CI) was determined by using data obtained from the X-ray diffractogram of cellulose, and the following equation (Segal, 1957):

$$CI = \frac{I_{200} - I_{am}}{I_{200}}$$

(I_{200} is the maximum intensity of the (200) lattice diffraction, and I_{am} is the intensity diffraction at 18° 2θ degrees).

The X-ray diffraction (XRD) analysis was performed on powder samples with a Rigaku Smart Lab diffractometer operating with a copper anode ($\lambda_{K\alpha}$=1.5418 Å). The diffractograms were recorded in the following conditions: generator voltage: 40 kV, tube current: 30 mA, scan step size: 0.05°, time/step 2 s.

For Fourier transform infrared (FT-IR) spectroscopy investigation, thin discs (study sample: 1 mg, KBr: 99 mg) were shaped, and analyzed with a Perkin Elmer 1725-x spectrophotometer functioning in the range of 4000-400 cm^{-1}. The PeakFit v4.12 software was used for IR bands deconvolution. The best curve fit was evaluated on the basis of the statistical parameters: R^2: correlation coefficient, SE: standard error, F-statistic: Fisher ratio.

Prepublished Article

https://doi.org/10.1180/clm.2024.6 Published online by Cambridge University Press

The relative quantities of metakaolin, zeolite and illite were determined on the basis the areas of their FT-IR bands. The areas were evaluated by means of the PeakFit software.

For thermal analysis, a SetaramSetsys 24 apparatus was used. The operating conditions were as follows: atmosphere: air, heating rate: 10 °C/min, reference material and crucible: alumina, sample masse: 78 mg

The microstructure of carbon-coated cured samples was investigated with TESCAN VEGA3 electron microscope, which was equipped with 20 mm^2 X-Max diffusion silicon detector.

The flexural strength (σ_{FS}) of the samples was evaluated with an EX 150 DeltaLab apparatus (loading rate: 12×10^{-3}kN/s) and using the following equation:

$$\sigma_{FS} = \frac{3F.L}{2bh^2}$$

(F: load at failure; L: distance between the two supports (2.8 cm) of the apparatus; b and h are the width and the thickness of the tested samples). The measurements were carried out in triplicate, and the standard deviations were in the range of 0.1-0.7 MPa.

The total porosity (P_T) of the samples was calculated according to the relation:

$$P_T = 100\left(1 - \frac{\rho_a}{\rho_t}\right)$$

(ρ_a and ρ_t are the apparent and true densities, which were measured by pycnometry method).

The maximum amount of water retained by the samples (saturation time: 5 min) was determined by weighting samples before and after contact with water. A water-submerged sponge was used as a source of water.

3. Results and discussion

3.1. Microstructure characterization

Based on the XRD traces given in Fig. 6, all cured alkali-activated samples were the object of the formation of zeolite ZK-14 (PDF #84-0693) and sodium carbonate (PDF # 86-0298). In line with the results of Valentini (2018), carbonation occurred in alkali-activated metakaolin samples. Referring to the latter author and to Zhang et al. (2014), carbonation was the result of the presence of excess Na ions in the pore solution, and it occurred according to the following reactions:

$CO_2(g) + 2OH^-(aq) \rightarrow CO_3^{2-}(aq) + H_2O$

$2Na^+(aq) + CO_3^{2-}(aq) + xH_2O \rightarrow Na_2CO_3 \cdot xH_2O\ (s)$.

Preprinted Article

https://doi.org/10.1180/clm.2024.6 Published online by Cambridge University Press

Referring once again to Fig. 6, the formation of hydrosodalite (PDF#76-1639) was suspected seeing that its main X-ray reflections (°2θ = 14.09 (6.286 Å), 24.53 (3.629 Å)) are overlapped with those of zeolite ZK-14 (°2θ = 14.02 (6.314 Å), 24.41 (3.646 Å)). According to Król et al. (2007) the formation of sodalite can be explained thermodynamically by higher stability of its denser lattice.

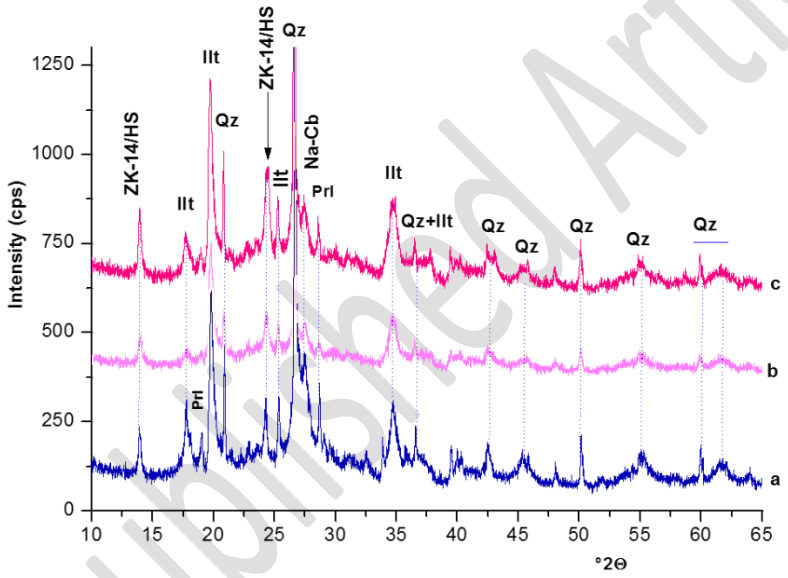

Fig. 6. X-ray diffraction patterns of the cured samples.
(a): cured cellulose-free samples ; (b): cured heated clay-5 mass% cellulose; (c): cured heated clay-10 mass% cellulose. ZK-14: Zeolite ZK-14 (PDF# 84-0698), IIt: Illite (PDF# 43-0685),Cb: Carbonate (PDF # 86-0298), HS: Hydrosodalite (PDF# 76-1639), Prl: Pyrophyllite (PDF# 96-0277), Qz: Quartz (PDF# 05-0490).

As expected, SEM examinations (Figs. 7&8) revealed pseudo-granular particles identified to hydrosodalite together with elongated particles associated with zeolite ZK-14 particles. A careful examination of the microstructure displayed hydrosodalite-free zones in the vicinity of zeolite ZK-14 particles. This fact could be related to the differences in the nucleation and the coalescence processes of these zeolites or to the elemental heterogeneity across the matrix. Discussion about zeolite formation is provided below.

Preprinted Article

https://doi.org/10.1180/clm.2024.6 Published online by Cambridge University Press

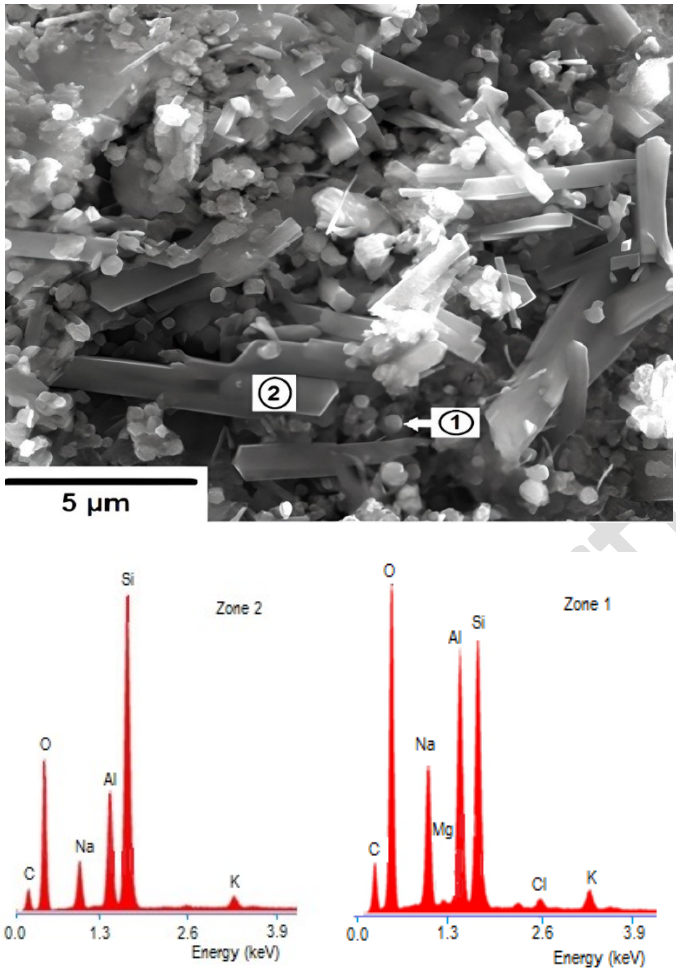

Fig. 7. Typical microstructure of the cured sample (10 mass% cellulose), and EDS spectra associated with hydrosodalite (zone 1) and zeolite ZK-14 (zone 2).

Preprint Article

https://doi.org/10.1180/clm.2024.6 Published online by Cambridge University Press

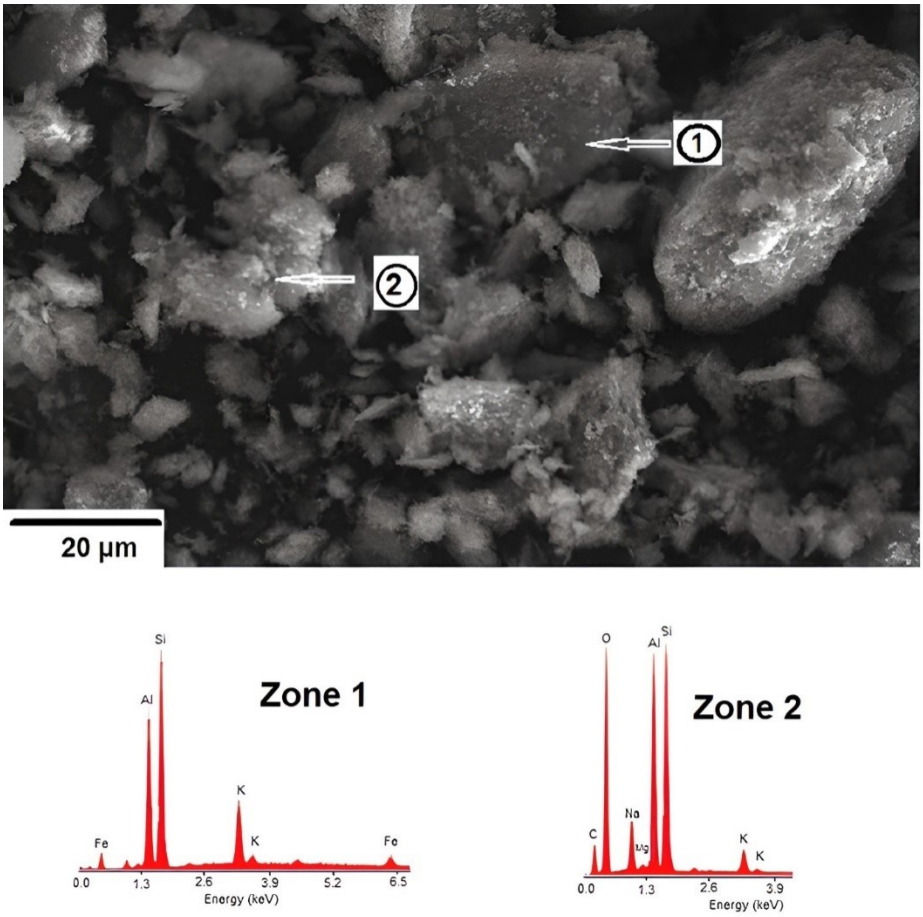

Fig. 8. SEM micrograph showing unreacted illite particle (Zone 1) and geopolymer-rich domain (Zone 2).

FT-IR analysis of the cured the samples displayed bands associated with metakaolin, illite, quartz and carbonate (Fig. 9). The zeolites/geopolymer bands could not be identified with certainty because of bands overlapping. So, the broad bands in the ranges of 3000-3700 cm^{-1} and 800-1400 cm^{-1} were deconvoluted (Fig. 10). The bands at 3504-3571, 958-946 cm^{-1} were associated with zeolites (El Hafid and Hajjaji, 2018; Mourak et al., 2021; El Hafid and Hajjaji, 2015; Hajjaji, 2014). Based on the areas of the FT-IR bands of zeolites, metakaolin and illite, the amounts of the two former minerals evolved antagonistically, whereas that of illite slightly declined as the cellulose content increased (Fig. 11). Owing to the fact that metakaolin is a precursor of zeolite (Maruoka et al., 2023; Khaled et al., 2023) the increase of the zeolite amount should be accompanied with the decrease of the metakaolin amount and vice-versa. The unexpected presence of metakaolin in the cured samples could be due to the limited access of OH^- ions to embedded metakaolin particles, and to the interaction between

Preprint

https://doi.org/10.1180/clm.2024.6 Published online by Cambridge University Press

OH^- ions and cellulose chains (mercerization reaction) (Okano and Sarko, 1985; Nishimura et al., 1991).

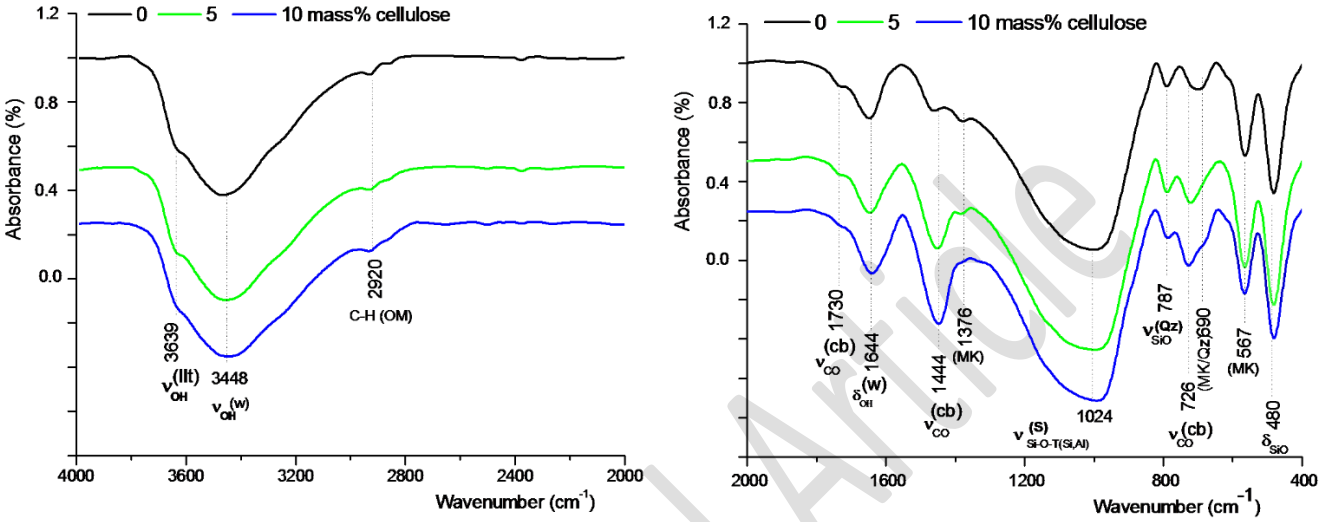

Fig. 9. FT-IR spectra of the cured cellulose-free sample (0 % mass cellulose) and cured cellulose-containing samples (5 and 10 mass% cellulose). For clarification reason, the O-H stretching vibration zone and the fingerprint region are separated.
MK: Metakaolin, S: Silicates, IIt: Illites, W: Water, cb: Carbonates, Qz: Quartz, OM: Organic matter.

Prepublished Article

https://doi.org/10.1180/clm.2024.6 Published online by Cambridge University Press

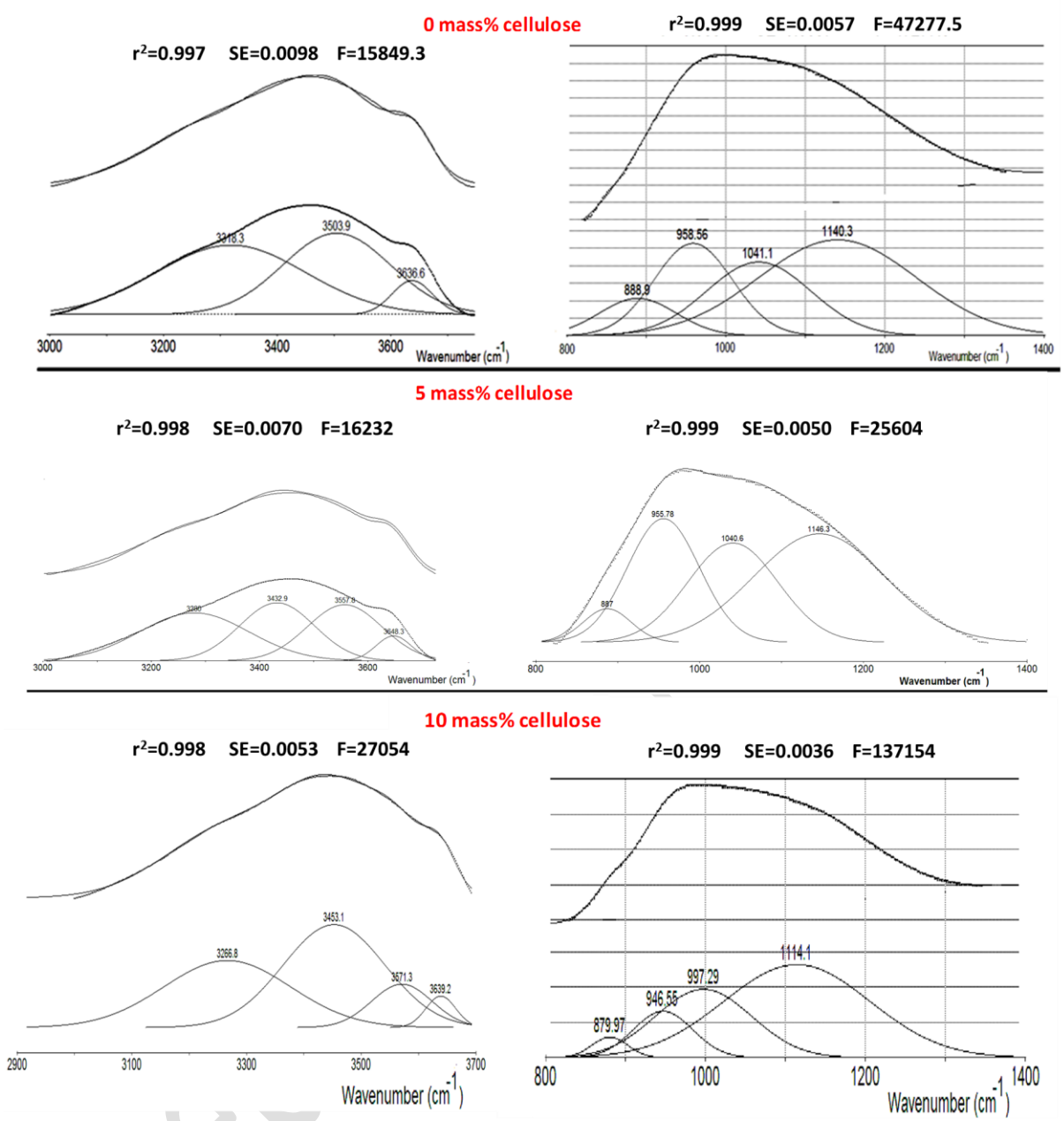

Fig. 10. Deconvolution plots of the broad FT-IR bands in the ranges of 3000-3700 cm^{-1} and 800-1400 cm^{-1}.

https://doi.org/10.1180/clm.2024.6 Published online by Cambridge University Press

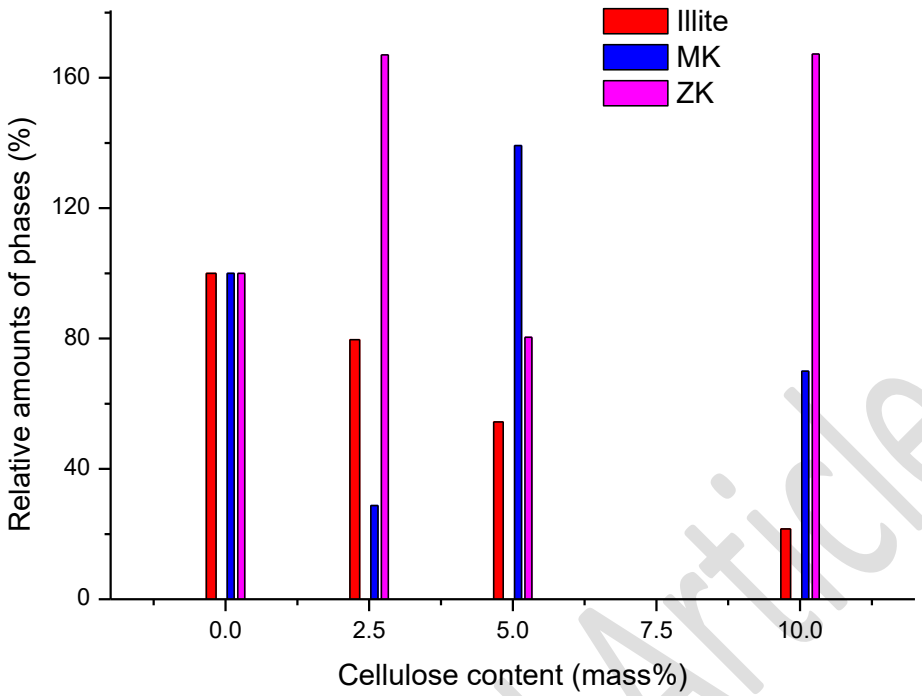

Fig. 11. Variation of the relative amounts of zeolite ZK-14 (ZK), metakaolin (MK) and illite as a function of cellulose content.

SEM examination showed that the microstructure of the cured samples was composed of zones such as seen in Fig. 12. The feature of such domains did not resemble to those of the above-identified zones, and their atomic ratios Al/Si were almost constant (about 1). In contrast, their (Na,K)/Si atomic ratios varied between (1.25; 0.6). In this respect, it is worth noting that the atomic ratios of Si/Al, Si/Na and Al/Na of the used material were 1.4, 1.0 and 0.74, respectively. It was believed that the aforementioned domains corresponded to the areas of geopolymer, that was consisted of poly(sialate) units (Al/Si = 1) (Chen et al., 2022; Zibouche et al., 2009). On the other hand, it should be noted that the geopolymer and hydrosodalite chemical compositions were somewhat close. Therefore, it could be assumed that geopolymer was a precursor for hydrosodalite formation.

Preprint Published Article

https://doi.org/10.1180/clm.2024.6 Published online by Cambridge University Press

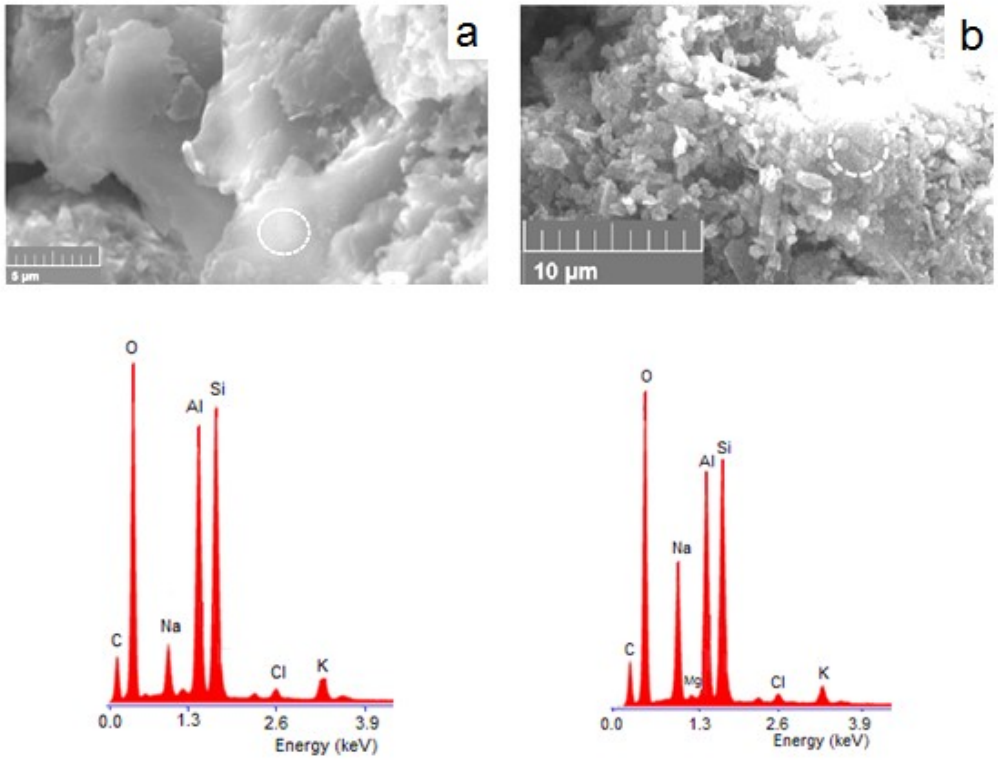

Fig. 12. SEM micrographs showing geopolymer-rich zones and their corresponding EDS spectra. (a): 0 mass% cellulose; (b): 10 mass% cellulose.

Considering the ternary diagram (SiO_2-Al_2O_3-Na_2O), which delimited the stability domains of zeolites, and the chemical composition of the cured cellulose-free sample for instance, the elemental representative point of the sample fell within the zeolite P domain (Fig. 13). The mismatch between the detected zeolites (zeolite ZK-14, hydrosodalite) and the expected one could be essentially due to the sample heterogeneity, and consequently to the difference in the spatial distribution of oxides. In fact, the formation of zeolite ZK-14 required a high amount of silica (about 63 mass%) and relatively low contents of Al_2O_3 (about 22.9 mass%) and Na_2O (about 14.1 mass%). In contrast, hydrosodalite is supposed to occur in matrix locations where the contents of silica, alumina and sodium oxide are below 19, 39 and 42 mass% respectively.

Preprint

https://doi.org/10.1180/clm.2024.6 Published online by Cambridge University Press

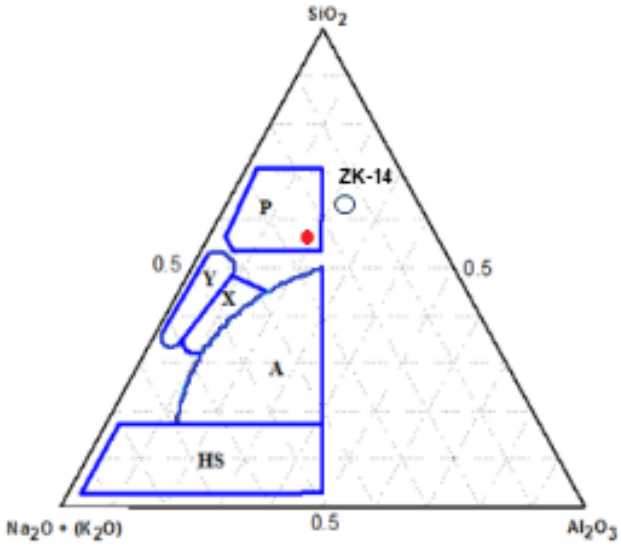

Fig. 13. Ternary diagram showing the stability domains of zeolites (P, Y, X, A and HS) (Xu et al. 2009). The location of the zeolite ZK-14 (ZK-14) is introduced. The representative point of the cured sample is red indicated.

3.2. Mechanical and physical properties

The flexural strength of the cured samples increased almost linearly with the increase of cellulose content (Fig. 14). Among the mechanisms, which could be involved in the strengthening process, one may mention the formation and the intensification of bonds between cellulose fibers and samples constituents, the homogenous distribution of the fibers and pores, and the porosity reduction (Mourak et al., 2021; Zheng et al., 2023; Ye et al., 2018).

In relation with the porosity influence on the mechanical strength of cured samples, the results indicated that porosity diminished with the augmentation of the cellulose amount (Fig. 14), and its evolution affected the flexural strength as follows:

$$\sigma_{FS}(MPa) = 5.39 - 5.47Ln(\frac{P_T - 18.3}{15}) \quad (R^2_{Adj} = 0.94)$$

Cellulose addition also resulted in samples densification (Fig.14). So, the compaction process played a key role in samples strengthening. Moreover, the co-presence of zeolite and geopolymers induces an increase of the mechanical strength as zeolite particles act as filler (Andrejkovičová et al., 2016).It was believed that the samples strengthening was essentially linked to the formation of hydrogen bonds between functional moieties of cellulose and active sites of the remaining samples constituents. In this connection, it was observed that the FT-IR band at 3504 cm^{-1}, which was associated with the stretching vibrations of OH of zeolite attached to the compensating charge Na^+ (Szostak, 1992), was the object of shifting as the

Preprinted Article

https://doi.org/10.1180/clm.2024.6 Published online by Cambridge University Press

cellulose addition increased (54 cm^{-1} and 67 cm^{-1} for samples with 5 and 10 mass% cellulose) (Fig. 10). Schematic representations of such a bond and hydrogen bondings between cellulose and the remaining constituents are provided in Fig. 15.

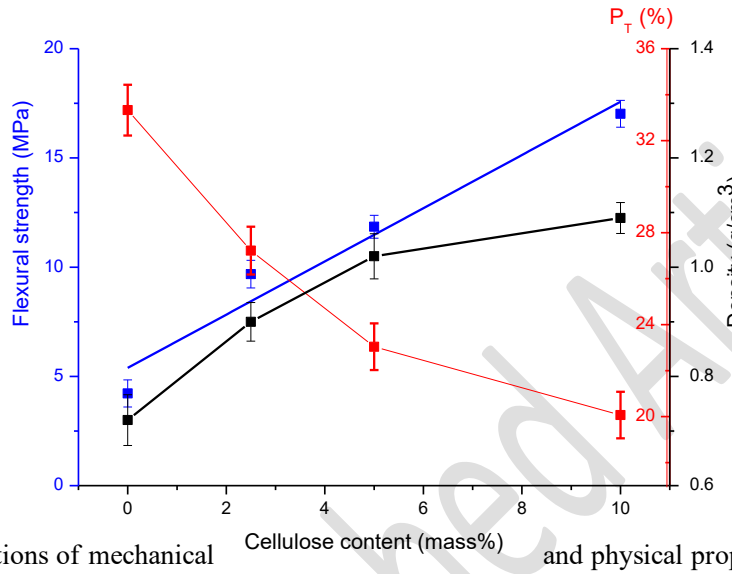

Fig. 14. Variations of mechanical and physical properties of the cured samples against cellulose content.

Prepublished Article

https://doi.org/10.1180/clm.2024.6 Published online by Cambridge University Press

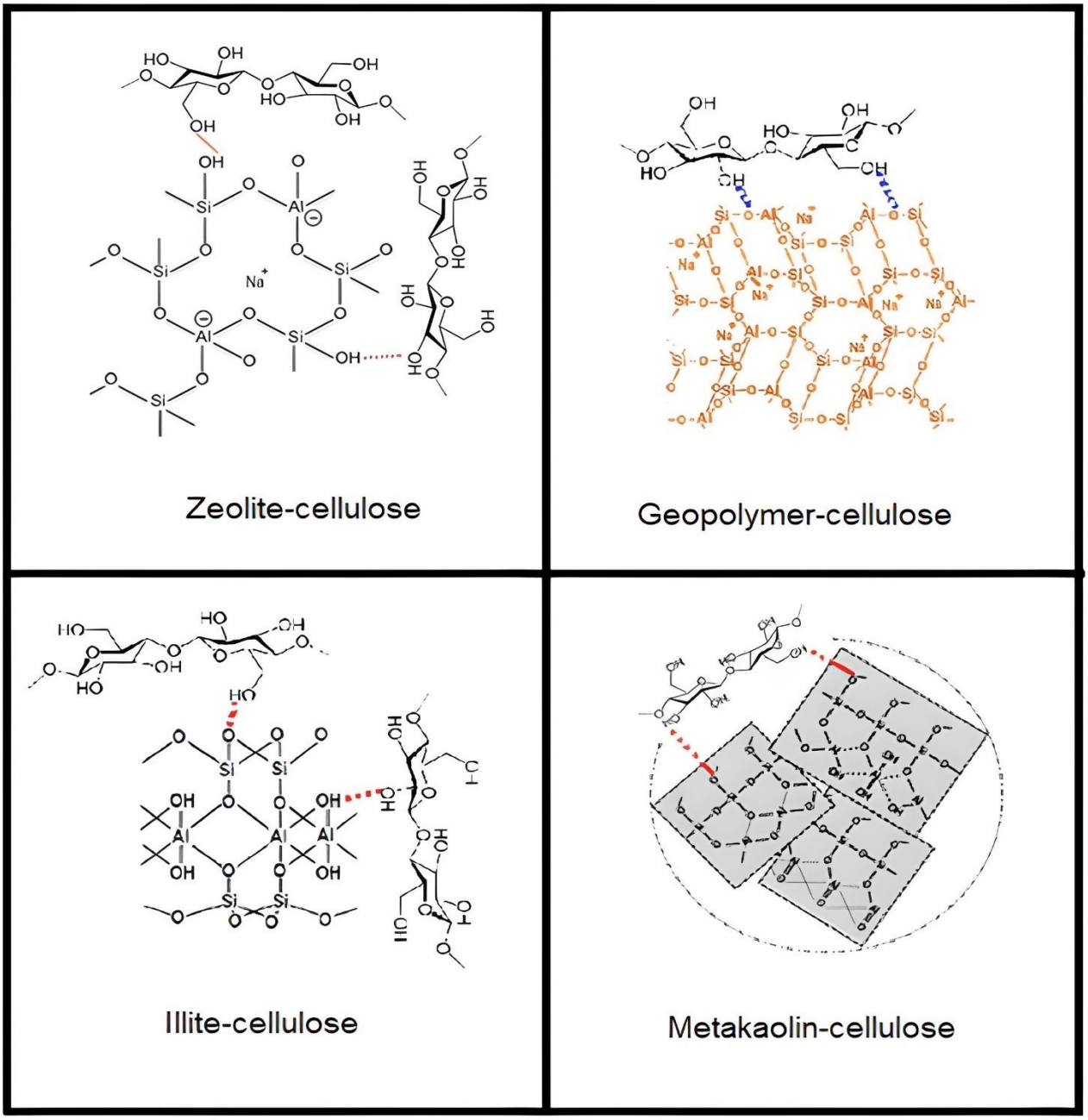

Fig. 15. Schematic representations of hydrogen bondings, which occurred between cellulose and cured samples constituents (zeolite, geopolymer, illite and metakaolin).

The rise of cellulose content led to the increase of water absorption as seen in Fig.16. This fact could not be associated with samples porosity because it was shown that porosity continuously decreased with the increase of the cellulose content. In this context, it was believed that the measured amount of adsorbed water was an average of the water amounts retained in the open and connected pores, and by zeolites, geopolymer and cellulose fibers.

https://doi.org/10.1180/clm.2024.6 Published online by Cambridge University Press

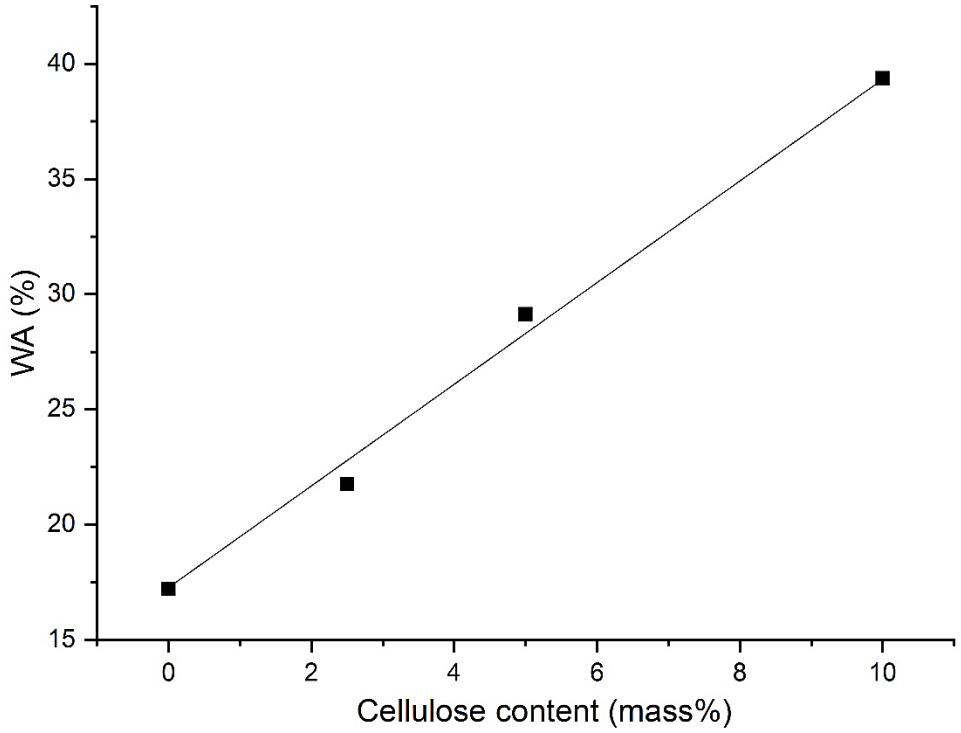

Fig. 16. Evolution of water absorption by the cured samples as a function of cellulose content.

The products obtained could be used as lightweight mortars as well as binders for bricks manufacturing. As compared with some natural fiber-reinforced geopolymer composites, the studied products had high flexural strength (Table 2).

Table 2. Flexural strength of some fiber-reinforced geopolymer composites.

Fiber	Flexural strength (MPa)	References
Cotton	5.85	Korniejenko et al. (2016)
Sisal	5.90	
Jute fibers	5.4	Silva et al. (2019)
Kenaf	6.08	Abbas et al. (2023)

https://doi.org/10.1180/clm.2024.6 Published online by Cambridge University Press

Sawdust	10.20	Duan et al. (2016)
Oil palm trunk	4.12	Kavipriya et al. (2021)
Carbon fiber	3.90-5.10	Nuaklong et al. (2021)
Cellulose	Up to 17	This study

4. Conclusion

The results of this study yielded the following conclusions:

i): Moroccan clay, which consisted of kaolinite, pyrophyllite and illite (main clay mineral), was thermally-activated by heating at 700°C for 2 hrs for geopolymer synthesis. Due to the heating, kaolinite was the object of dehydroxylation at about 523°C, whereas illite and pyrophyllite resisted heating up to about 900°C. The clay heating resulted in the formation of metakaolin, considered as a high-grade aluminosilicate, for the geopolymer preparation. The heated clay was mixed with cellulose (up to 10 mass%), which was extracted from the date palm (Phoenix dactylifera) rachis, and alkali-activated by NaOH solution (6 M). The samples prepared were cured at 83°C for 30 days under open atmosphere.

ii): As a result of curing, hydrosodalite, zeolite ZK-14, Na-carbonate and geopolymer composed of poly(sialate) units (Al/Si atomic ratio = 1) were formed. The formation of these compounds, which was in line with some reported studies dealing with the geopolymerization of fly ash- or metakaolin-based source materials, was discussed in relation with to the literature data.

iii): Metakaolin as well as illite were found in all studied samples. The change of the relative amounts of metakaolin and zeolites against cellulose addition evolved antagonistically, whereas that of illite slightly decreased. Zeolites were relatively abundant in the cured samples containing 2.5 and 10 mass% cellulose. On the other hand, it was believed that because of the low to moderate polymerization degree (892) of the cellulose, the fibers were well dispersed throughout the matrix because no bundle was observed at the SEM magnification (20 k) used.

iv): Cellulose addition improved the performances of the cured samples since it led to the increase of their mechanical strength, and to the reduction of their porosity. In addition, it resulted in their densification. Taking for instance the sample containing 10 mass% cellulose, the ratio strength/density was enhanced by about 17%. The performances improvement was

Prepublished Article

https://doi.org/10.1180/clm.2024.6 Published online by Cambridge University Press

mainly attributed to hydrogen bondings between the functional groups of cellulose and active sites of the formed aluminosilicate minerals as well as metakaolin.

v): As compared with some natural fiber-reinforced geopolymer composites, the studied cured mixtures had high mechanical strength. They could be used as lightweight mortars or as binders for bricks manufacturing.

References

Abbas A. G. N., Aziz F. N. A. A., Abdan K., Nasir N. A. M., Huseien G. F. (2023) Experimental evaluation and statistical modeling of kenaf fiber-reinforced geopolymer concrete. *Construction and Building Materials*, **367**, 130228.

Almutairi A.L., Tayeh B.A., Adesina A., Isleem H.F., Zeyad A.M. (2021) Potential applications of geopolymer concrete in construction: A review. Case Studies in Construction Materials, **15**, e00733.

Andrejkovičová S., Sudagar A., Rocha J., Patinha C., Hajjaji W., da Silva E.F., Velosa A., Rocha F. (2016) The effect of natural zeolite on microstructure, mechanical and heavy metals adsorption properties of metakaolin based geopolymers. *Applied Clay Science*, **126**, 141-152.

Aravindh M., Sathish S., Ranga Raj R., Karthick A., Mohanavel V., Patil P.P., Muhibbullah M., Osman S.M. (2022) A review on the effect of various chemical treatments on the mechanical properties of renewable fiber-reinforced composites. Advances in Materials *Science and Engineering*, **2022**.

Asyraf M.R.M., Syamsir A., Supian A.B.M., Usman F., Ilyas R.A., Nurazzi N.M., Norrrahim M.N.F., Razman M.R., Zakaria S.Z.S., Sharma S., Itam Z., Rashid M.Z.A. (2022) Sugar palm fibre-reinforced polymer composites: influence of chemical treatments on its mechanical properties. *Materials*, **15(11)**, 3852.

Ayub F., Khan S.A. (2023) An overview of geopolymer composites for stabilization of soft soils. *Construction and Building Materials*, **404**, 133195.

Bashline L., Lei L., Li S., Gu Y. (2014) Cell wall, cytoskeleton, and cell expansion in higher plants. *Molecular plant*, **7(4)**, 586-600.

Chen S., Wang K., Wei E., Muhammad Y., Yi M., Wei Y., Fujita T. (2022) Preparation of Al_2O_3-$2SiO_2$/geopolymer powder by hydrolytic sol-gel method and its activity characterization and research on the reaction mechanism. *Powder Technology*, **397,** 117026.

Preprint Article

https://doi.org/10.1180/clm.2024.6 Published online by Cambridge University Press

Chen X., Wang K., Wang Z., Zeng H., Yang T., Zhang X. (2021) Highly stretchable composites based on cellulose. *International Journal of Biological Macromolecules*, **170**, 71-87.

da Silva Rego J.H., Sanjuán M.Á., Mora P., Zaragoza A., Visedo G. (2023) Carbon dioxide uptake by brazilian cement-based materials. *Applied Sciences*, **13(18)**, 10386.

de Souza L.O., Liebscher M., de Souza L.M.S., de Andrade Silva F., Mechtcherine V. (2023) Effect of microcrystalline and nano-fibrillated cellulose on the mechanical behavior and microstructure of cement pastes. *Construction and Building Materials*, **408**, 133812.

dos Reis R.R., Effting C., Schackow A. (2023) Cellulose nanofibrils on lightweight mortars for improvement of the performance of cement systems. *Carbohydrate Polymer Technologies and Applications*, **5**, 100303.

Duan P., Yan C., Zhou W., Luo W. (2016) Fresh properties, mechanical strength and microstructure of fly ash geopolymer paste reinforced with sawdust. *Construction and Building Materials*, **111**, 600-610.

El Hafid K., Hajjaji M. (2015) Effects of the experimental factors on the microstructure and the properties of cured alkali-activated heated clay. *Applied Clay Science*, **116**, 202-210.

El Hafid K., Hajjaji M. (2018) Geopolymerization of glass-and silicate-containing heated clay. *Construction and Building Materials*, **159**, 598-609.

Emenike E.C., Iwuozor K.O., Saliu O.D., Ramontja J., Adeniyi A.G. (2023) Advances in the extraction, classification, modification, emerging and advanced applications of crystalline cellulose: A Review. *Carbohydrate Polymer Technologies and Applications*, **6**, 100337.

Etale A., Onyianta A.J., Turner S.R., Eichhorn S.J. (2023) Cellulose: a review of water interactions, applications in composites, and water treatment. *Chemical Reviews*, **123(5)**, 2016-2048.

Evans R., Wallis A. F. (1989) Cellulose molecular weights determined by viscometry. *Journal of applied polymer science*, ***37*(8),** 2331-2340.

Farhan K.Z., Johari M.A.M., Demirboğa R. (2021) Impact of fiber reinforcements on properties of geopolymer composites: A review. *Journal of Building Engineering*, **44**, 102628.

Ferreira S.R., Ukrainczyk N., e Silva K.D.D.C., Silva L.E., Koenders E. (2021) Effect of microcrystalline cellulose on geopolymer and Portland cement pastes mechanical performance. *Construction and Building Materials*, **288**, 123053.

Giacobello F., Ielo I., Belhamdi H., Plutino M.R. (2022) Geopolymers and functionalization strategies for the development of sustainable materials in construction industry and cultural heritage applications: A Review. *Materials*, **15(5),** 1725.

https://doi.org/10.1180/clm.2024.6 Published online by Cambridge University Press

Gualtieri A.F., Ferrari S. (2006) Kinetics of illite dehydroxylation. Physics and Chemistry of Minerals, **33**, 490-501.

Hajjaji M. (2014) Minéralogie et transformation thermique des matériaux argileux de la région de Marrakech, Maroc. *Comunicaçõe Geológicas*, **101(1).**

Hallac B. B., Ragauskas A. J. (2011) Analyzing cellulose degree of polymerization and its relevancy to cellulosic ethanol. *Biofuels, Bioproducts and Biorefining*, **5(2),** 215-225.

Heah C. Y., Kamarudin H., Al Bakri A. M., Binhussain M., Luqman M., Nizar I. K. Ruzaidi C.M., Liew Y. M. (2011) Effect of curing profile on kaolin-based geopolymers. *Physics Procedia*, **22**, 305-311.

Jaberizadeh M.M., Danoglidis P.A., Shah S.P., Konsta-Gdoutos M.S. (2023) Eco-efficient cementitious composites using waste cellulose fibers: Effects on autogenous shrinkage, strength and energy absorption capacity. *Construction and Building Materials*, **408**, 133504.

Jamshaid H., Mishra R.K., Raza A., Hussain U., Rahman M.L., Nazari S., Chandan V., Muller M., Choteborsky R. (2022) Natural cellulosic fiber reinforced concrete: influence of fiber type and loading percentage on mechanical and water absorption performance. Materials, **15(3)**, 874.

Jwaida Z., Dulaimi A., Mashaan N., Othuman Mydin M.A. (2023) Geopolymers: The Green Alternative to Traditional Materials for Engineering Applications. *Infrastructures*, **8(6),** 98.

Kavipriya S., Deepanraj C. G., Dinesh S., Prakhash N., Lingeshwaran N., Ramkumar S. (2021) Flexural strength of Lightweight geopolymer concrete using sisal fibres. *Materials Today: Proceedings*, **47**, 5503-5507.

Khaled Z., Mohsen A., Soltan A., Kohail M. (2023) Optimization of kaolin into Metakaolin: Calcination Conditions, mix design and curing temperature to develop alkali activated binder. *Ain Shams Engineering Journal*, **14(6)**, 102142.

Korniejenko K., Frączek E., Pytlak E., Adamski M. (2016) Mechanical properties of geopolymer composites reinforced with natural fibers. *Procedia Engineering*, **151**, 388-393.

Król M., Rożek P., Mozgawa W. (2017) Synthesis of the sodalite by geopolymerization process using coal fly ash. *Pol. J. Environ. Stud*, **26(6),** 2611-2617.

Lazorenko G., Kasprzhitskii A., Mischinenko V., Kruglikov A. (2022) Fabrication and characterization of metakaolin-based geopolymer composites reinforced with cellulose nanofibrils. *Materials Letters*, **308**, 131146.

Published Article

https://doi.org/10.1180/clm.2024.6 Published online by Cambridge University Press

Malešič J., Kraševec I., Kralj Cigić I. (2021) Determination of cellulose degree of polymerization in historical papers with high lignin content. *Polymers*, **13(12),** 1990.

Maruoka L.M., Pinheiro I.F., Freitas H.S., Nobre F.X., Scalvi L.V. (2023) Effect of thermal annealing on kaolin from the Amazon region, aiming at the production of geopolymer. *Journal of Materials Research and* Technology, **25**, 2471-2485.

Mijarsh M. J. A., Johari M. M., Ahmad Z. A. (2015) Effect of delay time and Na_2SiO_3 concentrations on compressive strength development of geopolymer mortar synthesized from TPOFA. *Construction and Building Materials*, **86**, 64-74.

Mo B. H., Zhu H., Cui X. M., He Y., Gong S. Y. (2014) Effect of curing temperature on geopolymerization of metakaolin-based geopolymers. *Applied clay science*, **99**, 144-148.

Mohamad N., Muthusamy K., Embong R., Kusbiantoro A., Hashim M.H. (2022) Environmental impact of cement production and Solutions: A review. *Materials Today: Proceedings*, **48**, 741-746.

Mourak A., Hajjaji M., Alagui A. (2021) Cured alkali-activated heated clay-cellulose composites: Microstructure, effect of glass addition and performances. *Boletín de la Sociedad Española de Cerámica y Vidrio*, **60(1)**, 62-72.

Nishimura H., Okano T., Sarko A. (1991) Mercerization of cellulose. 5. Crystal and molecular structure of Na-cellulose I. Macromolecules, **24(3)**, 759-770.

Nuaklong P., Wongsa A., Boonserm K., Ngohpok C., Jongvivatsakul P., Sata V., Sukontasukkul P., Chindaprasirt P. (2021) Enhancement of mechanical properties of fly ash geopolymer containing fine recycled concrete aggregate with micro carbon fiber. *Journal of Building Engineering*, **41**, 102403.

Okano T., Sarko A. (1985) Mercerization of cellulose. II. Alkali–cellulose intermediates and a possible mercerization mechanism. Journal of Applied Polymer Science, **30(1)**, 325-332.

Raghunath S., Hoque M., Foster E.J. (2023) On the Roles of Cellulose Nanocrystals in Fiber Cement: Implications for Rheology, Hydration Kinetics, and Mechanical Properties. *ACS Sustainable Chemistry & Engineering*, **11(29)**, 10727-10736.

Ranjbar N., Kuenzel C., Spangenberg J., Mehrali M. (2020) Hardening evolution of geopolymers from setting to equilibrium: A review. *Cement and Concrete Composites*, **114**, 103729.

Santana H.A., Júnior N.S.A., Ribeiro D.V., Cilla M.S., Dias C.M. (2021) Vegetable fibers behavior in geopolymers and alkali-activated cement based matrices: A review. *Journal of Building Engineering*, **44**, 103291.

https://doi.org/10.1180/clm.2024.6 Published online by Cambridge University Press

Segal L.G. J. M. A., Creely J. J., Martin Jr A. E., Conrad C. M. (1959) An empirical method for estimating the degree of crystallinity of native cellulose using the X-ray diffractometer. *Textile research journal*, **29(10),** 786-794.

Semugaza G., Mielke T., Castillo M. E., Gierth A. Z., Tam J. X., Nawrath S., Lupascu D. C. (2023) Reactivation of hydrated cement powder by thermal treatment for partial replacement of ordinary portland cement. *Materials and Structures*, **56(3)**, 48.

Shi W., Sha Z., Qiao F., Tang W., Luo C., Zheng Y., Wang C., Ge J. (2023) Study on the temporal and spatial evolution of china's carbon dioxide emissions and its emission reduction path. *Energies*, **16(2)**, 829.

Silva G., Salirrosas J., Ruiz G., Kim S., Nakamatsu J., Aguilar R. (2019) Evaluation of fire, high-temperature and water erosion resistance of fiber-reinforced lightweight pozzolana-based geopolymer mortars. In IOP Conference Series: Materials Science and Engineering.**706 (1),** 012016. IOP Publishing.

Singh H., Gupta R. (2020) Influence of cellulose fiber addition on self-healing and water permeability of concrete. *Case Studies in Construction Materials*, **12**, e00324.

Sotelo-Piña C., Aguilera-González E.N., Martínez-Luévanos A. (2019) Geopolymers: Past, present, and future of low carbon footprint eco-materials. *Handbook of Ecomaterials*, **4**, 2765-85.

Szostak R. (1992). In Handbook of Molecular Sieves Van Nostrand Reinhold. New York.

Tanu H.M., Unnikrishnan S. (2022) Utilization of industrial and agricultural waste materials for the development of geopolymer concrete-A review. *Materials Today: Proceedings*, **65**, 1290-1297.

Valentini L. (2018) Modeling dissolution–precipitation kinetics of alkali-activated metakaolin. *ACS omega*, **3(12)**, 18100-18108.

Van Deventer J. S. J., Provis J. L., Duxson P., Lukey G. C. (2007) Reaction mechanisms in the geopolymeric conversion of inorganic waste to useful products. *Journal of hazardous materials*, **139(3)**, 506-513.

Van Jaarsveld J. G. S., Van Deventer J. S., Lukey G. C. (2002) The effect of composition and temperature on the properties of fly ash-and kaolinite-based geopolymers. *Chemical Engineering Journal*, **89(1-3),** 63-73.

Weng L., Sagoe-Crentsil K. (2007) Dissolution processes, hydrolysis and condensation reactions during geopolymer synthesis: Part I—Low Si/Al ratio systems. *Journal of materials science*, **42**, 2997-3006.

https://doi.org/10.1180/clm.2024.6 Published online by Cambridge University Press

Ye H., Zhang Y., Yu Z., Mu J. (2018) Effects of cellulose, hemicellulose, and lignin on the morphology and mechanical properties of metakaolin-based geopolymer. *Construction and Building Materials*, **173**, 10-16.

Zhang J., Yang H., Zhang S., Feng T., Li Y. (2023) Potential utilization of CO_2 foams in developing lightweight building materials. *Journal of Building Engineering*, **76**, 107342.

Zhang Z., Provis J. L., Reid A., Wang H. (2014) Fly ash-based geopolymers: The relationship between composition, pore structure and efflorescence. *Cement and concrete research*, **64**, 30-41.

Zheng Y., Wang Z., Wan Z., Yang X., Lin F., Chen Y., Tang L., Lin G., Lu B. (2023) Mechanochemical fabrication of geopolymer composites based on the reinforcement effect of microfibrillated cellulose. *Ceramics International*, **49(1)**, 503-511.

Zibouche F., Kerdjoudj H., de Lacaillerie J. B. D. E., Van Damme H. (2009) Geopolymers from Algerian metakaolin. Influence of secondary minerals. *Applied Clay Science*, **43(3-4),** 453-458.

Prepublished Article

https://doi.org/10.1180/clm.2024.6 Published online by Cambridge University Press